ACS central science

Research Article

Cite This: ACS Cent. Sci. 2019, 5, 1584−1590

http://pubs.acs.org/journal/acscii

Solution Catalytic Cycle of Incompatible Steps for Ambient Air Oxidation of Methane to Methanol

Benjamin S. Natinsky, Shengtao Lu, Emma D. Copeland, Jason C. Quintana, and Chong Liu*

Department of Chemistry and Biochemistry, University of California, Los Angeles, California 90025, United States

Supporting Information

ABSTRACT: Direct chemical synthesis from methane and air under ambient conditions is attractive yet challenging. Low-valent organometallic compounds are known to activate methane, but their electron-rich nature seems incompatible with O_2 and prevents catalytic air oxidation. We report selective oxidation of methane to methanol with an O_2-sensitive metalloradical as the catalyst and air as the oxidant at room temperature and ambient pressure. The incompatibility between C−H activation and O_2 oxidation is reconciled by electrochemistry and nanomaterials, with which a concentration gradient of O_2 within the nanowire array spatially segregated incompatible steps in the catalytic cycle. An unexpected 220 000-fold increase of the apparent reaction rate constants within the nanowire array leads to a turnover number up to 52 000 within 24 h. The synergy between nanomaterials and organometallic chemistry warrants a new catalytic route for CH_4 functionalization.

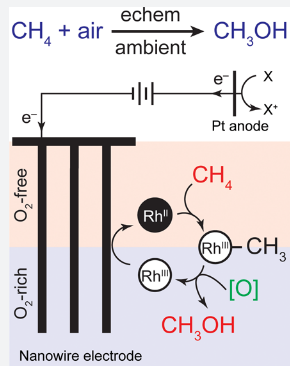

INTRODUCTION

It is attractive to directly use air and natural gas, mostly methane (CH_4), as raw materials for the synthesis of methanol (CH_3OH),[1−4] an important commodity chemical. High-valent, electron-deficient organometallic compounds have been attempted as the centers for C−H activation and the immediate oxidants, presuming that the metal complexes can be reoxidized by air to fulfill a catalytic cycle.[5−8] Because of the low reactivity of its C−H bond, CH_4 functionalization proceeds at elevated temperatures which incurs possible overoxidation into other products.[9−11] Alternatively, electron-rich organometallic compounds are capable of selectively activating CH_4 at low temperature.[2,4,12] This intrigues us to establish a hypothetical catalytical cycle at ambient conditions, in which a reductive or homolytic step of CH_4 activation is followed by air oxidation to yield CH_3OH with minimal overoxidation. However, as the step of CH_4 activation may not be favored thermodynamically and O_2 can oxidatively quench the catalytic species (Figure 1A), external energy input is needed for catalyst regeneration, and a spatial control of these incompatible reactions is required.

In biology, incompatible biochemical reactions coexist within one organelle by localizing conflicting reactions. One example is the fixation of dinitrogen (N_2) in aerobic bacteria (Figure 1B). O_2-sensitive nitrogenase for N_2 fixation is powered by the reducing equivalents generated from the tricarboxylic acid (TCA) cycle with O_2 as the terminal electron acceptor.[13] The tandem reactions of aerobic respiration and N_2 fixation are only possible with the buildup of an O_2 gradient, where the O_2-sensitive nitrogenase is positioned in a local anaerobic part of cytoplasm and the TCA cycle in an aerobic one.[14] Inspired by the strategies employed in biology, we propose that in order to fulfill a catalytic cycle, the steps of C−H activation and air oxidation should be connected for the catalysis yet spatially separated with mitigated oxidative quenching (Figure 1C). While these requirements are challenging in a homogeneous solution, we posit that they can be satisfied with the use of a nanowire array electrode and electrochemistry. When an electrode is biased at a potential more negative than the redox potentials of O_2 and the catalyst, redox-active catalysts can be regenerated by electrochemistry.[15] Moreover, the electrochemical reduction of O_2 will establish a local O_2 gradient in the solution near the electrode surface. This effect is much more pronounced for nanomaterials and porous electrodes in general,[16,17] effectively creating an O_2-free domain within nanomaterials suitable for chemical steps incompatible with O_2. In support of this argument, our previous work demonstrated that a nanowire array electrode can create an O_2-free domain that allows anaerobic microbial reduction of CO_2.[16] Establishing a similar O_2 gradient and regenerating the CH_4-activating catalyst with electrochemically active nanowires (Figure 1C), here we report a catalytic cycle for ambient air oxidation of CH_4 to CH_3OH with O_2-sensitive, electron-rich Rh^{II} tetramesityl porphyrin metalloradical, $(TMP)Rh^{II}$ (**1a**, Figure 2A), as the catalyst.[18−20]

RESULTS AND DISCUSSION

At ambient conditions, 2 equiv of **1a** reversibly activate 1 equiv of CH_4 with a large equilibrium constant ($K = 2.2 \times 10^5$ at 298 K), which yields the methylated and hydride species ($(TMP)Rh{-}CH_3$, **1b**; $(TMP)Rh{-}H$, **1c**, respectively) (Figure 2A).[19] The sterically bulky TMP ligand and the requirement of a four-centered transition state warrant a selectivity toward

Received: June 27, 2019
Published: August 1, 2019

DOI: 10.1021/acscentsci.9b00625
ACS Cent. Sci. 2019, 5, 1584−1590

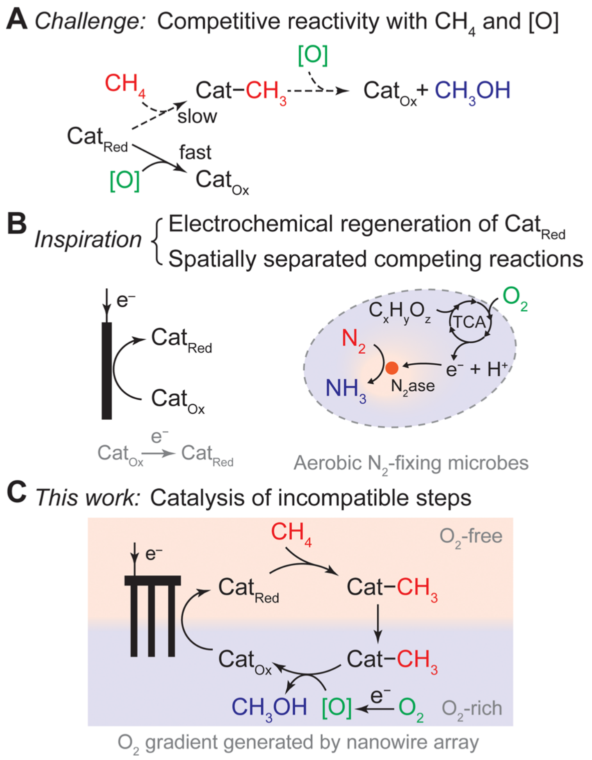

Figure 1. Motivation toward a catalytic cycle for ambient air oxidation of CH_4 to CH_3OH. (A) The incompatibility of low-valent, electron-rich organometallic compounds for CH_4 functionalization with O_2-derived oxidants ([O]). (B) The inspirations to address such an incompatibility from examples in biology and (C) the proposed approach reported in this work.

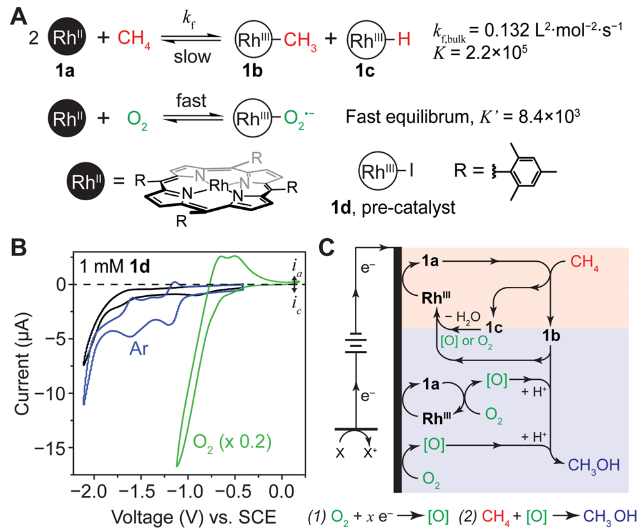

Figure 2. Electrochemical characterization and proposed catalytic cycle utilizing $(TMP)Rh^{II}$, **1a**, as the catalyst. (A) The reactivities of Rh^{II} metalloradical with CH_4 and O_2. (B) Cyclic voltammograms of 1 mM **1d** with 0.1 M $TBAClO_4$ in 1,2-DFB under Ar (blue) and air (green) environment. Black, blank solution without **1d**. 100 mV/s; Pt working electrode for blank and in Ar, glassy carbon electrode in O_2. The current in O_2 is multiplied by a factor of 0.2. (C) Schematic of the proposed catalytic cycle with **1d** as the precatalyst. Upon CH_3OH formation, Rh^{III} is generated whose charge is balanced by the perchlorate anion (ClO_4^-) in solution, which has been omitted for clarity. Oxidant [O] signifies reactive oxygen species such as hydrogen peroxide and superoxide. The proposed reaction is displayed below the catalytic cycle. x = 2.1 on average based on experimental data (entries 2–6 in Table S1).

CH_4 by two orders of magnitude versus other larger substrates including CH_3OH.[21] However, in a homogeneous solution, such a reactivity with CH_4 is not translatable to catalysis when paired with oxidants such as O_2. **1a** and O_2 react to form a Rh^{III} superoxo species under a fast equilibrium ($K' = 8.4 \times 10^3$ at 298 K, Figure 2A),[22] and this reaction outcompetes the kinetically slow process of CH_4 activation ($k_{f,bulk} = 0.132$ $M^{-2} \cdot s^{-1}$ at 296 K).[19] Despite this, we argue that electrochemistry can regenerate **1a** in situ from its oxidized counterparts thereby potentially allowing the activation of CH_4 with **1a** in air. Rh^{III} tetramesityl porphyrin iodide ((TMP)Rh–I, **1d**) was synthesized based on literature (Figure S1).[19] In an argon (Ar) environment and noncoordinating solvent, 1,2-difluorobenzene (1,2-DFB),[23] with 0.1 M tetrabutylammonium perchlorate ($TBAClO_4$), a cyclic voltammogram (CV) of **1d** on a platinum (Pt) working electrode displays quasi-reversible behavior at an electrode potential $E_{appl} = -1.26$ V vs standard calomel electrode (SCE) (Figure 2B), consistent with a previous report that the Rh^{II} species can be regenerated by electrochemistry.[24,25] In the presence of O_2, a catalytic cathodic wave was observed on a glassy carbon electrode preceding the Rh^{III}/Rh^{II} redox couple ($E_{appl} < -0.7$ V vs SCE) (green trace in Figure 2B), while the CV trace in the absence of **1d** yielded no such activity (Figure S2). Previous literature report the generation of superoxide and peroxide as the immediate products both in solution or electrochemically when O_2 and Rh^{II} porphyrin are in a stoichiometric ratio.[22,26,27] Here our experimental data in air suggest that additional catalytic irreversible reduction of O_2 is feasible when the amount of O_2 is in surplus.

The capability of generating reactive oxygen species [O] electrochemically with Rh porphyrin leads us to explore whether those [O] can activate **1b** and yield CH_3OH. Stoichiometric reactions between different hydroperoxide species and **1b**, a stable compound prepared in air (Figure S3), were performed at a 1:1 ratio under ambient conditions (see Supporting Information). The reaction between *t*-butyl hydroperoxide and **1b** was tracked via ^1H NMR and indicated the formation of CH_3OH at the expense of the methyl group in **1b** (Figure S4). This suggests that the methylated species **1b** is capable of releasing CH_3OH by hydroperoxide. Moreover, we found that a 3-h electrolysis of **1b** at $E_{appl} = -1.4$ V vs SCE yielded a stoichiometric amount of CH_3OH (Table S1, entry 1). A gas chromatograph equipped with a mass spectrometer (GC-MS), allowing for a clear separation of electrolyte and catalyst from product determination, was used to detect the product after establishing a calibration curve (Figure S5). This indicates that the electrochemically generated [O] from O_2 reduction can be a serendipitous oxidant which yields CH_3OH after the step of CH_4 activation. During the aforementioned electrolysis, on average 2.3 equiv of electrons are consumed per CH_3OH molecule synthesized, indicating that [O] is possibly of a hydroperoxide nature. However, not all of the generated [O] will lead to CH_3OH formation, conveying that the value of 2.3 electrons acts as an upper boundary for the reaction during electrolysis.

Given the literature and our experimental data, we propose to establish a solution catalytic cycle of incompatible reactions at ambient conditions in air (Figure 2C), which is impossible in homogeneous solution but potentially feasible when

DOI: 10.1021/acscentsci.9b00625
ACS Cent. Sci. 2019, 5, 1584–1590

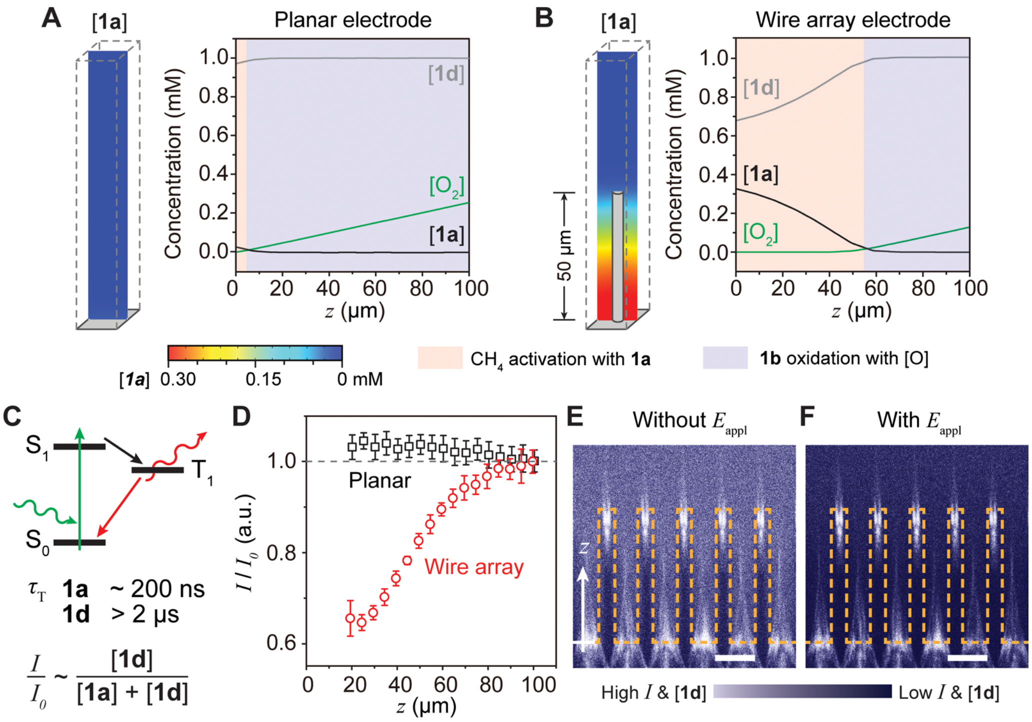

Figure 3. Numerical simulations and experimental validation of a microscopic concentration gradient for CH_4 activation. (A, B) Simulated concentration gradients of O_2, **1a**, and **1d** ([O_2], [**1a**], and [**1d**], respectively) near a planar (A) and wire array (B) electrode. z, distance away from electrode surface; E_{appl} = −1.5 V vs SCE. (C) Jablonski diagram illustrating potential phosphorescence emission of **1a** and **1d**. The triplet state lifetime (τ_T) of **1a** is much shorter than the one of **1d**. I/I_0, normalized emission intensity of phosphorescence. (D) Experimentally determined I/I_0 versus z for planar (black) and wire array (red). 0.1 mM **1d** in the bulk solution, 0.1 M $TBAClO_4$ in 1,2-DFB, E_{appl} = −1.5 V vs SCE. (E, F) The corresponding cross-sectional heatmaps of unnormalized phosphorescence intensity without (E) and with (F) E_{appl}. The surface of the Si wire array is delineated in yellow. Scale bar, 15 μm.

combining electrochemistry and nanomaterials. A silicon (Si) nanowire array was proposed to offer a similar and even enhanced effect as that of a porous electrode with respect to induced concentration gradients.[16,17] By utilizing nanowire array morphology as the working electrode in the presence of **1d** and O_2, the oxidant [O] will be electrochemically generated in situ from O_2 with the creation of an O_2 gradient. The created O_2 gradient enables a nanoscopic separation of incompatible reaction steps. In a localized anaerobic environment near the base of the wire array (pink area in Figure 2C), electrochemically regenerated **1a** activates CH_4 and yields **1b**, which diffuses out and oxidatively hydroxylates to yield CH_3OH in the aerobic region (blue area in Figure 2C).

Numerical simulations based on electrochemistry models support the feasibility of the proposed catalytic cycle in the wire array. Finite-element simulations using the COMSOL Multiphysics program were conducted for different electrode geometries based on the experimentally available information (see Supporting Information),[16,17] including the fast electrochemical equilibrium of Rh^{III}/Rh^{II} redox couple, the reported chemical reactivities,[19,22] and the molecular diffusion coefficients determined by diffusion ordered spectroscopy (DOSY) with ^1H nuclear magnetic resonance (NMR) (Figure S6). Figure 3A displays the calculated concentrations of **1a**, **1d**, and O_2, denoted as [**1a**], [**1d**], and [O_2], respectively, versus the distance away from electrode surface (z) on a planar electrode at E_{appl} = −1.4 V vs SCE. An anaerobic domain of predominantly CH_4-reactive **1a**, pink colored in Figure 3A, is minimal as compared to the extensive aerobic domain (light blue) where CH_4-unreactive **1d** is predominant. In contrast, for an exemplary wire array of 50 μm length, 4 μm diameter, and 15 μm periodicity (i.e., distance between adjacent wires) under the same condition, an extended anaerobic region is visible toward the base of the array and potentially favors CH_4 activation (Figure 3B). These results support our hypothesis that a nanowire array electrode can spatially define an anaerobic region for CH_4 activation, which is microscopically adjacent to an aerobic one ready for CH_3OH formation. Variation of the physical parameters such as the reactivities between O_2 and **1a** as well as the charge-transfer rate of O_2 reduction (Figure S7) does not alter the effectiveness of the wire array for establishing concentration gradients, indicating the robustness of this design.

Spatially resolved optical measurements confirmed the predicted concentration gradients of **1a** and **1d** within the wire array electrode. The Si wire array, used as a model system, was prepared by reactive ion etching after photolithography (Figure S8, Supporting Information).[28] The geometry was based on the same one used in the numerical simulation (Figure 3B) to help validate the conclusions drawn from the simulations. Electrochemical characterizations suggest that the prepared Si wire arrays are electrochemically active toward O_2 reduction with the presence of **1d** (Figure S9). As the lifetime of the excited triplet (τ_T) for **1d** (>2 μs) is much longer than the one of **1a** (∼200 ns),[24] under optical excitation **1d** exhibits much stronger phosphorescence emission from 630 to 750 nm as compared to **1a** (Figure S10). Thus, in a mixed solution containing both **1a** and **1d**, the local concentration percentage of **1d**, and subsequently the percentage of **1a**, can be tracked by monitoring the phosphorescence intensity after normalizing

DOI: 10.1021/acscentsci.9b00625
ACS Cent. Sci. 2019, 5, 1584−1590

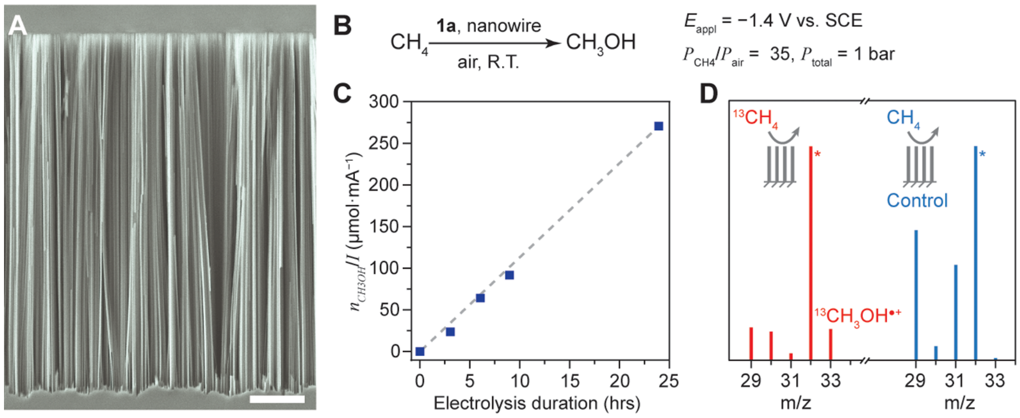

E	CH_4	C_2H_6	C_3H_8	$PhCH_3$
C−H BDE (kcal/mol)	105	101	101 (1°), 99 (2°)	88 (CH_3)
Product	CH_3OH	C_2H_5OH	OH (> 99%)	$PhCH_2OH$
TON (avg in solution)	0.37	1.49	0.32 (1°)	1.22
TON' (avg in array)	2972	11968	2570	9799
$k_{f,nano}$ ($L^2 \cdot mol^{-2} \cdot s^{-1}$)	2.9×10^4	9.3×10^3	1.0×10^3	9.1×10^3
$k_{f,bulk}$ ($L^2 \cdot mol^{-2} \cdot s^{-1}$)	0.132	−	−	0.0104

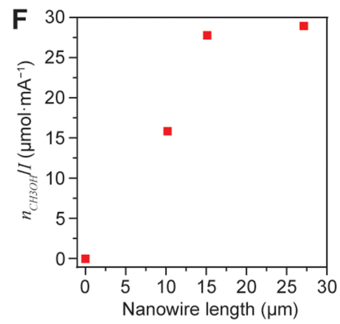

Figure 4. Ambient air oxidation of alkanes to primary alcohols enabled by nanomaterials and electrochemistry. (A) Si nanowire array imaged by a scanning electron microscope. Scale bar, 2 μm. (B) General conditions used for catalytic ambient air CH_4 oxidation to CH_3OH. (C) The amount of generated CH_3OH normalized to the average electric current (n_{CH_3OH}/I), as a function of the electrolysis duration. (D) Mass spectra for the electrolyte solution after 3-h bulk electrolysis. Red, $^{13}CH_4$ as the substrate; blue, CH_4 of natural isotope abundance. (E) Catalytic reactivities for different alkane substrates. BDE, bond dissociation energy; TON, turnover number based on catalyst in solution; TON′, turnover number based on catalyst in reaction layer; $k_{f,nano}$ and $k_{f,bulk}$, kinetic rate constants of C−H activation by **1a** calculated in nanowire array and reported in the literature,[19] respectively. (F) The relationship between n_{CH_3OH}/I in a 3-h electrolysis and the lengths of nanowire array. A planar electrode was considered as an array of 0 μm wire length.

to the intensity when only **1d** is in the solution (I/I_0) (Figure 3C). An electrochemical setup was constructed under a confocal microscope with 526 nm excitation to in situ map the phosphorescence intensity near the electrode surface in air (Figure S11, Supporting Information). Figure 3D displays the values of I/I_0 at different z values for both planar (black) and wire array (red) Si electrodes when E_{appl} = −1.5 V vs SCE. Near a planar electrode, the values of I/I_0 remain constant, and it suggests that the local concentration of **1d** was not significantly perturbed (Figures 3D and S12). For a Si wire array (Figure S8) that possesses the exact same geometry simulated in Figure 3B,[28] the values of I/I_0 decrease toward the base of wire array, indicating a local depletion of **1d** and subsequently an accumulation of **1a**. The accumulation of CH_4-reactive **1a** is also suggested in the steady-state cross-sectional heatmaps of phosphorescence. A distinguishably lower emission intensity profile was observed when E_{appl} = −1.5 V vs SCE in the wire array (Figure 3E), as compared to the case at the open-circuit condition (Figure 3F). The fidelity between simulation (Figure 3A,B) and experimental results (Figure 3E,F) confirms that the wire array spatially generates an O_2-free domain in air with a localized accumulation of **1a**, which is reactive toward ambient CH_4 activation.

Selective ambient air oxidation of CH_4 to CH_3OH was observed with **1d** as the precatalyst when E_{appl} = −1.4 V vs SCE on a Si wire array electrode. A Si nanowire array, prepared by electroless wet etching, with a wire length of ∼15 μm and diameter of ∼100 nm (Figure 4A),[29] was applied as the working electrode for a three-electrode configuration in a customized electrochemical reactor (Figure S13). A gas mixture with a defined ratio between CH_4 and air (P_{CH4}/P_{air}) was delivered at a constant rate under ambient pressure. In a 1,2-DFB solution of 1 mM **1d** and P_{CH_4}/P_{air} = 35, a 3-h bulk electrolysis on a Si nanowire electrode (E_{appl} = −1.4 V vs SCE) yielded 0.37 ± 0.20 mM CH_3OH (n = 3, Figure 2B, Table S1, entry 2). The observed CH_3OH can be directly attributed to the reactivity of **1a** and not the platinum (Pt) counter electrode as a similar performance is observed when a graphitic carbon cloth is substituted as the counter electrode (Table S1, entry 3). Longer electrolysis up to 24 h led to a higher concentration of CH_3OH up to 6.45 ± 0.92 mM (Table S1, entries 4−6). Since experimentally there was some fluctuation of electrochemical current as the electrolysis was conducted at a constant potential, a fairer comparison between experiments of different durations is based on the moles of CH_3OH normalized to the average electrochemical current. The CH_3OH yield normalized by the current (n_{CH_3OH}/I) is a near linear function of the electrolysis duration (Figure 4C), which suggests a continuous catalytic reaction without much catalyst degradation. On average, 2.1 ± 0.3 equiv of electrons, a value averaged based on entries 2−6 in Table S1, corresponds to the formation of 1 equiv of CH_3OH. The calculated value in the bulk electrolysis of **1d** in a CH_4/air mixture is lower than the theoretical value of 4 should hydroperoxide be the only

DOI: 10.1021/acscentsci.9b00625
ACS Cent. Sci. 2019, 5, 1584−1590

reactive oxygen species. This suggests that reactive oxygen species other than hydroperoxide, such as superoxide, likely contribute to the oxidation of **1b** and the formation of CH_3OH. As hydroperoxide is known to react reversibly with **1a** in a similar fashion as O_2,[30] a spatial distribution of reactive oxygen species generated by the O_2 also contributes to the observed reactivity. Interestingly, no other C_1 or C_2 liquid products were observed, and the generation of CO or CO_2 was not detectable in the outgas by GC-MS (Figure S14). While overoxidation may pose an issue since **1a** is known to activate CH_3OH,[17] the absence of other products but CH_3OH formation in the electrolysis suggests a strong selectivity for CH_4, possibly due to the 100-times faster rate of CH_4 activation as compared to CH_3OH by **1a**,[21,31] as well as the relatively high solubility of CH_4 in the solvent (9.54 mM at 1 bar CH_4 based on ^1H NMR).

Electrolysis in the absence of either **1d**, air, or CH_4 led to the disappearance of CH_3OH formation (Table S1, entries 7−9, respectively). Introducing ^{13}C-labeled CH_4 as the substrate in lieu of the one with natural ^{13}C abundance resulted in the surge of m/z = 33 peak in the mass spectrum (Figure 4D, Table S1, entry 10). This suggests the formation of a $^{13}CH_3OH^{\bullet +}$ fragment in the spectrum from the yielded $^{13}CH_3OH$ (Figure S15). Our observations are consistent with a selective catalysis of CH_3OH formation with CH_4 as the substrate and O_2 as the oxidant. The turnover number (TON), defined as the ratio between product concentration and the concentration of precatalyst **1d** in solution, was calculated to be 0.37 for the 3-h electrolysis and 6.45 for the 24-h electrolysis (Figure 4E and Table S1). Such a definition of TON values obviates the fact that only the catalyst molecules within the nanowire array are responsible for CH_4 activation in our proposed mechanism. Therefore, we also calculated an alternative turnover number (TON′), which is defined as the ratio between the moles of generated product and the moles of **1d** precatalyst within the nanowire array. This TON′ relevant to electrochemical catalysis[15] was found to be 2972 for the 3-h electrolysis and up to 51 807 for a 24-h experiment (Figure 4E and Table S1). The calculated values of turnover numbers are comparable to those reported values of other catalysts for CH_4 functionalization (Tables S2 and S3), while our process is operating at room temperature and ambient pressure with air as the oxidant and CH_3OH as the product.

We further applied this ambient catalytic system to other substrates including ethane (C_2H_6), propane (C_3H_8), and toluene ($PhCH_3$). In all cases, selective oxidation to primary alcohols was observed (Table S1, entries 11−13), and their corresponding TON and TON′ are shown in Figure 4E. When *t*-butylbenzene was introduced as the substrate, no oxidation products were observed, which is in line with a previous report about the reactivity of Rh^{II} porphyrin species[32] (Table S1, entry 14). The reaction kinetics for different substrates was also compared in the developed catalytic system. As catalytic reactions of different substrates were conducted under different substrate concentrations in solution (see Supporting Information), the observed kinetic rate constants other than the turnover numbers were employed for evaluation. Given that the step of C−H activation is shown to be turnover-limiting (vide infra), we calculated the rate constants of C−H activation in a nanowire array, $k_{f,nano}$, based on the observed rate of alcohol accumulation (Figure 4E). Despite the large differences of bond dissociation energies (BDE) of the cleaved C−H bonds (Figure 4E), $k_{f,nano}$, which is independent of substrate concentration, appears to decrease even as BDE is simultaneously decreasing. Such a dependence of $k_{f,nano}$ over different substrates conveys the significant effect of steric constraint from **1a** as reported before.[18,19]

Electrochemically generated **1a** is the active species for CH_4 activation, and the nanowire array is responsible for **1a**'s sustained presence and activity in air. We found that halving the concentration of **1d** in bulk electrolysis led to a decrease of reaction rate by 4.3 times (Table S1, entry 15). This is consistent with the second-order kinetics on **1a** for CH_4 activation (Figure 2A) and implies that C−H activation is turnover-limiting in the proposed catalytic cycle (Figure 2A). When we substituted the precatalyst **1d** in the bulk electrolysis with a Rh^{III} octaethyl porphyrin iodide ((OEP)Rh-I, **2**) synthesized based on the literature (Figure S16),[33] no CH_3OH was produced (Table S1, entry 16). While **2** exhibits a similar electrochemical response as **1d** with a slight shift of redox potential (Figure S17), the less bulky OEP supporting ligand is reported to favor the formation of the $[(OEP)Rh^{II}]_2$ dimer, which is unreactive toward CH_4.[18] The observed difference of reactivities between **1d** and **2** as precatalysts suggests that it is the electrochemically generated **1a** that activates CH_4. Moreover, the catalytic ambient air oxidation of CH_4 to CH_3OH stopped, and no CH_3OH was observed when the nanowire array electrode was replaced with a planar wireless electrode, a wire array with larger spacing among wires, or an increased O_2 partial pressure at P_{CH4}/P_{air} = 1 (Table S1, entry 17, 18, and 19, respectively). Such observations are indeed consistent with our simulation results that a higher concentration of O_2, planar wireless electrode, or a less dense nanowire array all mitigate the anaerobic domain, the population of **1a**, and thereby the reactivity toward CH_4 (Figure S18). Moreover, on the other hand, a 3-h electrolysis with P_{CH_4}/P_{air} > 1000 yielded 0.25 mM CH_3OH (Table S1, entry 20), illustrating the existence of a fine window of O_2 partial pressure, which will result in optimal CH_3OH generation. These control experiments also indirectly support previous reports regarding the incompatibility of **1a** with the O_2 in air.[22]

Along the same lines, the effect of nanowire length was also investigated to ascertain its role in catalysis and CH_3OH formation. Additional nanowire arrays of 10 and 27 μm in length were prepared (Figure S19). The yields of CH_3OH for a 3-h electrolysis were 0, 0.19 (Table S1, entry 21), 0.37, and 0.45 (Table S1, entry 22) for a planar electrode and nanowires of 10, 15, and 27 μm, respectively. The corresponding n_{CH_3OH}/I values are plotted as a function of nanowire length in Figure 4F. As the length of the nanowire increases, the anaerobic domain in which C−H activation occurs expands, resulting in accelerated catalysis and subsequently more CH_3OH formation. Such an increase of reaction rate plateaued between nanowires of 15 and 27 μm in length, suggesting that the system reached the intrinsic limit based on its mechanism, and an additional length of nanowire is not beneficial for reaction productivity anymore. Lastly, a spent nanowire electrode, defined as a nanowire array that was previously utilized for a CH_3OH-yielding electrolysis, exhibited no activity toward CH_4 (Table S1, entry 23), and measurement of X-ray photoelectron spectroscopy (Figure S20) found no residual Rh species on the nanowire's surface after electrolysis. It shows that the catalytic system is robust with minimal catalyst degradation, and any

DOI: 10.1021/acscentsci.9b00625
ACS Cent. Sci. 2019, 5, 1584−1590

possible Rh nanoparticle formation on the surface of the nanowires is not responsible for the observed reactivity.

Interestingly, the rate of CH_4 activation by **1a** was significantly increased in the nanowire array as compared to the one in bulk solution. $k_{f,nano} = 2.9 \times 10^4$ $L^2 \cdot mol^{-2} \cdot s^{-1}$ for CH_4 activation, about 220 000 times the value in bulk solution ($k_{f,bulk} = 0.132$ $L^2 \cdot mol^{-2} \cdot s^{-1}$).[19] A similar enhancement, by a factor of about 870 000, was observed when toluene was the substrate. As the C−H activation step of **1a** undergoes an entropically disfavored four-centered transition state,[18,19] high concentration and favorable orientation between two Rh centers will increase the reaction kinetics of CH_4 activation.[21] We speculated that the negative charges from the native oxide on the Si nanowire's surface as well as the relatively low dielectric constant of 1,2-DFB[23] promote the adsorption of precatalyst **1d** near the nanowire's surface. While this effect will not alter the reactivity between **1a** and O_2 as suggested in our experiments (comparing entry 2, 19, and 20 in Table S1), it will lead to a high local concentration of **1a**, potentially create favorable intermolecular orientation between neighboring Rh centers, and subsequently increase its rate of CH_4 activation. Such a putative argument is supported by the observation that the rate of CH_3OH formation was minimal when the negative charges on the Si surface were passivated with terminal trimethylsilyl groups[34] (Table S1, entry 24). It implies that confining homogeneous organometallic reactions within the space of a nanowire array can accelerate the reaction rate significantly, an effect possibly similar to the one observed when an organometallic catalyst is encapsulated in a supramolecular cavity.[35] Overall, the introduction of electrochemistry and nanomaterials enables a catalytic ambient air oxidation of CH_4 to CH_3OH with the use of a low-valent electron-rich organometallic compound that is otherwise unsuitable as a catalyst in a homogeneous solution. The concept of spatially separating incompatible reaction steps at the nanoscale for a complete catalytic cycle provides new options for designing catalysis for a broad range of chemical transformations.

■ ASSOCIATED CONTENT

Supporting Information

The Supporting Information is available free of charge on the ACS Publications website at DOI: 10.1021/acscentsci.9b00625.

Full experimental details, detailed synthetic procedures, electrochemical characterizations, numerical simulation, product quantification, and additional tables and figures (PDF)

■ AUTHOR INFORMATION

Corresponding Author

*E-mail: chongliu@chem.ucla.edu.

ORCID

Benjamin S. Natinsky: 0000-0002-3046-6667

Chong Liu: 0000-0001-5546-3852

Author Contributions

C.L. supervised the project. C.L. and B.S.N. designed experiments and wrote the paper. B.S.N. synthesized the compounds with the assistance from E.D.C. and J.C.Q. B.S.N. conducted electrochemical characterizations and product quantification. L.S. conducted numerical simulations and experiments of confocal microscopy. All the authors discussed the results and assisted during the manuscript preparation.

Notes

The authors declare no competing financial interest.

■ ACKNOWLEDGMENTS

We would like to acknowledge Greg Khitrov for the use of GC-MS, Xun Guan for the SEM images, Manisha Swain from the Kwon Group for synthesizing 2-(1-hydroperoxy-1-methoxyethyl)-5-methylcyclohexan-1-ol, and Paula Diaconescu for constructive discussions. We thank the Molecular Instrumentation Center lab at the University of California, Los Angeles for sample characterizations. E.D.C. acknowledges the UCLA undergraduate summer research program; C.L. acknowledges the startup fund from the University of California, Los Angeles and the financial support of the Jeffery and Helo Zink Endowed Professional Development Term Chair.

■ REFERENCES

(1) Gunsalus, N. J.; et al. Homogeneous Functionalization of Methane. *Chem. Rev.* **2017**, *117*, 8521−857.

(2) Labinger, J. A.; Bercaw, J. E. Understanding and exploiting C-H bond activation. *Nature* **2002**, *417*, 507−514.

(3) Caballero, A.; Perez, P. J. Methane as raw material in synthetic chemistry: the final frontier. *Chem. Soc. Rev.* **2013**, *42*, 8809−8820.

(4) Shilov, A. E.; Shul'pin, G. Activation and Catalytic Reactions of Saturated Hydrocarbons in the Presence of Metal Complexes. In *Activation of C-H Bonds by Low-Valent Metal Complexes ("The Organometallic Chemistry")*; Kluwer Academic Publishers, 2002; pp 127−129.

(5) Periana, R. A.; et al. A Mercury-Catalyzed, High-Yield System for the Oxidation of Methane to Methanol. *Science* **1993**, *259*, 340−343.

(6) Periana, R. A.; et al. Platinum Catalysts for the High-Yield Oxidation of Methane to a Methanol Derivative. *Science* **1998**, *280*, 560−564.

(7) Jones, C.; et al. Selective Oxidation of Methane to Methanol Catalyzed, with C−H Activation, by Homogeneous, Cationic Gold. *Angew. Chem.* **2004**, *116*, 4726−4729.

(8) O'Reilly, M. E.; Kim, R. S.; Oh, S.; Surendranath, Y. Catalytic Methane Monofunctionalization by an Electrogenerated High-Valent Pd Intermediate. *ACS Cent. Sci.* **2017**, *3*, 1174−1179.

(9) Latimer, A. A.; Kakekhani, A.; Kulkarni, A. R.; Nørskov, J. K. Direct Methane to Methanol: The Selectivity−Conversion Limit and Design Strategies. *ACS Catal.* **2018**, *8*, 6894−6907.

(10) Schwarz, H. Chemistry with Methane: Concepts Rather than Recipes. *Angew. Chem., Int. Ed.* **2011**, *50*, 10096−10115.

(11) Labinger, J. A. Selective alkane oxidation: hot and cold approaches to a hot problem. *J. Mol. Catal. A: Chem.* **2004**, *220*, 27−35.

(12) Janowicz, A. H.; et al. Oxidative addition of soluble iridium and rhodium complexes to carbon-hydrogen bonds in methane and higher alkanes. *Pure Appl. Chem.* **1984**, *56*, 13−23.

(13) Dixon, R.; Kahn, D. Genetic regulation of biological nitrogen fixation. *Nat. Rev. Microbiol.* **2004**, *2*, 621−631.

(14) Tsoy, O. V.; Ravcheev, D. A.; Čuklina, J.; Gelfand, M. S. Nitrogen Fixation and Molecular Oxygen: Comparative Genomic Reconstruction of Transcription Regulation in Alphaproteobacteria. *Front. Microbiol.* **2016**, *7*, 1343.

(15) Savéant, J. M. *Elements of Molecular and Biomolecular Electrochemistry: An Electrochemical Approach to Electron Transfer Chemistry*; John Wiley & Sons, Inc., 2006.

(16) Liu, C.; et al. Nanowire−Bacteria Hybrids for Unassisted Solar Carbon Dioxide Fixation to Value-Added Chemicals. *Nano Lett.* **2015**, *15*, 3634−3639.

(17) Newman, J. S.; Tobias, C. W. Theoretical Analysis of Current Distribution in Porous Electrodes. *J. Electrochem. Soc.* **1962**, *109*, 1183−1191.

DOI: 10.1021/acscentsci.9b00625
ACS Cent. Sci. 2019, 5, 1584−1590

(18) Sherry, A. E.; Wayland, B. B. Metalloradical activation of methane. *J. Am. Chem. Soc.* **1990**, *112*, 1259−1261.
(19) Wayland, B. B.; Ba, S.; Sherry, A. E. Activation of methane and toluene by rhodium(II) porphyrin complexes. *J. Am. Chem. Soc.* **1991**, *113*, 5305−5311.
(20) Thompson, S. J.; Brennan, M. R.; Lee, S. Y.; Dong, G. Synthesis and applications of rhodium porphyrin complexes. *Chem. Soc. Rev.* **2018**, *47*, 929−981.
(21) Zhang, X.-X.; Wayland, B. B. Rhodium(II) Porphyrin Bimetalloradical Complexes: Preparation and Enhanced Reactivity with CH_4 and H_2. *J. Am. Chem. Soc.* **1994**, *116*, 7897−7898.
(22) Cui, W.; Wayland, B. B. Superoxo, Peroxo, and Hydroperoxo Complexes Formed from Reactions of Rhodium Porphyrins with Dioxygen: Thermodynamics and Kinetics. *J. Am. Chem. Soc.* **2006**, *128*, 10350−10351.
(23) O'Toole, T. R.; Younathan, J. N.; Sullivan, B. P.; Meyer, J. T. 1,2-Difluorobenzene: a relatively inert and noncoordinating solvent for electrochemical studies on transition-metal complexes. *Inorg. Chem.* **1989**, *28*, 3923−3926.
(24) Vitols, S. E.; Friesen, D. A.; Williams, D. S.; Melamed, D.; Spiro, T. G. Excited State Dynamics of Rh(II) Tetramesityl Porphyrin Monomer from Nanosecond Transient Absorption and Emission Spectroscopy. *J. Phys. Chem.* **1996**, *100*, 207−213.
(25) Grass, V.; Lexa, D.; Momenteau, M.; Savéant, J.-M. Reductive Electrochemistry of Rhodium Porphyrins. Disproportionation of Intermediary Oxidation States. *J. Am. Chem. Soc.* **1997**, *119*, 3536−3542.
(26) Wayland, B. B.; Newman, A. R. Dioxygen and nitric oxide complexes of rhodium porphyrins. *Inorg. Chem.* **1981**, *20*, 3093−3097.
(27) Anderson, J. E.; Yao, C. L.; Kadish, K. M. Electroreduction of the dioxygen adduct of rhodium tetraphenylporphyrin: (TTP)Rh-(O_2). *Inorg. Chem.* **1986**, *25*, 3224−3228.
(28) Liu, C.; Tang, J.; Chen, H. M.; Liu, B.; Yang, P. A Fully Integrated Nanosystem of Semiconductor Nanowires for Direct Solar Water Splitting. *Nano Lett.* **2013**, *13*, 2989−2992.
(29) Huang, Z.; Geyer, N.; Werner, P.; de Boor, J.; Gösele, U. Metal-Assisted Chemical Etching of Silicon: A Review. *Adv. Mater.* **2011**, *23*, 285−308.
(30) Choi, K. S.; Lai, T. H.; Lee, S. Y.; Chan, K. S. Reduction of Rhodium (III) Porphyrin Hydroxide to Rhodium(II) Porphyrin. *Organometallics* **2011**, *30*, 2633−2635.
(31) Cui, W.; Wayland, B. B. Activation of C−H/H−H Bonds by Rhodium(II) Porphyrin Bimetalloradicals. *J. Am. Chem. Soc.* **2004**, *126*, 8266−8274.
(32) Del Rossi, K. J.; Wayland, B. B. Formation and thermal reactions of rhodium-carbon bonds derived from the reactions of octaethylporphyrin-rhodium(III) dimer with alkyl carbon-hydrogen bonds in alkyl aromatics. *J. Am. Chem. Soc.* **1985**, *107*, 7941−7944.
(33) Collman, J. P.; Boulatov, R. Synthesis and Reactivity of Porphyrinatorhodium(II)−Triethylphosphine Adducts: The Role of PEt_3 in Stabilizing a Formal Rh(II) State. *J. Am. Chem. Soc.* **2000**, *122*, 11812−11821.
(34) Plummer, J. D.; Deal, M. D.; Griffin, P. B. *Silicon VLSI Technology: Fundamentals, Practice and Modeling*; Prentice Hall, Inc., 2000.
(35) Fiedler, D.; Leung, D. H.; Bergman, R. G.; Raymond, K. N. Selective Molecular Recognition, C−H Bond Activation, and Catalysis in Nanoscale Reaction Vessels. *Acc. Chem. Res.* **2005**, *38*, 349−358.

DOI: 10.1021/acscentsci.9b00625
ACS Cent. Sci. 2019, 5, 1584−1590